JOURNAL OF Materials CHEMISTRY

Shape and size determination for zinc–aluminium–chloride layered double hydroxide crystallites by analysis of X-ray diffraction line broadening

Abdelali Ennadi,†[a] Ahmed Legrouri,*[b] André De Roy[c] and Jean Pierre Besse[c]

[a]*Laboratoire de Chimie-Physique, Faculté des Sciences Semlalia, Université Cadi Ayyad, B.P. 2390, Marrakech 40001, Morocco*
[b]*School of Science & Engineering, Al Akhawayn University, PO Box 1871, Ifrane 53000, Morocco. E-mail: a.legrouri@alakhawayn.ma*
[c]*Laboratoire des Matériaux Inorganiques, UPRES-A 6002, Université Blaise Pascal, 63177 Aubière-Cedex, France*

Received 26th April 2000, Accepted 4th July 2000
First published as an Advanced Article on the web 17th August 2000

The Rietveld method, extended by a Fourier analysis of line profiles on the basis of the Warren–Averbach method, has been used for analysing the powder X-ray diffraction (PXRD) pattern of a [Zn–Al–Cl] layered double hydroxide, in order to separate size and strain effects. Assuming a given size distribution (Cauchy) and an adjustable strain variation in space, this method allows the simultaneous determination of structural parameters and the size and strain parameters of the sample. The shape, size, size distribution and orientation of the crystallites are determined. It is found that the shape is markedly anisotropic and compatible with plate-like crystallites with a hexagonal symmetry; the structure being described in the $R\bar{3}m$ space group. The strain parameter, *i.e.* the distribution of atomic positions around their equilibrium positions, varies by a factor of 2 while the mean particle size changes from 120 Å to 2200 Å in the [001] and [110] directions, respectively. Such shape and size are in good agreement with the transmission electron microscopy (TEM) observations.

Introduction

Layered double hydroxides (LDHs) form a class of compounds related to clays.[1–5] They can be represented by the general formula: $[M^{II}_{1-x}M^{III}_{x}(OH)_2]^{x+}[X^{m-}_{x/m}\cdot nH_2O]^{x-}$, abbreviated as $[M^{II}$–M^{III}–X] (M^{II} and M^{III} = metal cations, X^{m-} = anion). They are built up of cationic $M(OH)_2$ brucite-like layers intercalated by anionic species. According to this formula, it is possible to obtain a wide range of such compounds by changing the nature and proportions of metallic cations in the main hydroxylated layers and by intercalation of a great number of solvated anions.

The most common natural counterpart of LDHs is the hydrotalcite group of minerals. The structure was first elucidated by Allmann[6,7] for the [Mg–Fe–CO_3] system (pyroaurite and sjögrenite) and by Brown *et al.*[8,9] for the [Mg–Al–CO_3] system (hydrotalcite and manasseite).

The distance between two adjacent layers depends mainly on the nature of the interlayer species and their electrostatic interaction with the main layers. The layers and an interlayer can be arranged in many different ways (1H, 2H, 3R, …) leading to hexagonal or rhombohedral symmetry.[7,10–13]

The object of this work is to determine the lattice strains and to present a better understanding of [Zn–Al–Cl] crystallite morphology from PXRD data. This information is of fundamental importance in studies of catalysts and can help understand thermal decomposition and other solid-state reactions such as grafting.[14,15] In this perspective, we have applied a multi-pattern version of the Rietveld program as modified by Le Bail[16,17] in order to take into account the line broadening due to size and strain effects. This method is based on the Warren–Averbach procedure[18,19] for separating size and strain effects.

Experimental

Materials

The compounds were prepared by the salt–oxide method.[20–22] All the reagents were of analytical grade and water was deionized and decarbonated in order to avoid carbonate intercalation in the LDH. A molar $AlCl_3$ solution was slowly added to an aqueous suspension of ZnO, under vigorous stirring, at room temperature. The pH of the mixture was monitored during the addition of aqueous $AlCl_3$. Each addition was observed to cause a pH decrease followed by a return to the initial pH value due to the buffering effect of ZnO. The end of the reaction was evidenced by the pH value, which remained constant after further addition of aqueous $AlCl_3$. The solid compound obtained was separated by centrifugation and washed with water. Chemical analyses of the [Zn–Al–Cl] phase confirmed the definite ratio Zn/Al = 2, which corresponds to the following composition for the phase obtained: $[Zn_{0.66}Al_{0.33}(OH)_2]^{0.33+}[Cl_{0.33}\cdot 0.66H_2O]^{0.33-}$.

Methods

PXRD patterns were recorded with a Siemens D501 diffractometer equipped with a graphite back-monochromator, using ($CuK_{\alpha 1}+CuK_{\alpha 2}$). The sample was passed through an 80 μm sieve in order to avoid preferential orientation during the structure determination. Using the McMurdie method,[23] the sample holder was rotated at a speed of 30 rpm. The data were collected in the 5–105° (2θ) range with a 0.04° (2θ) step and a 40 s per step counting time. The subtraction of the background was made before any further calculation.

TEM observations were carried out with a JEOL 120CX

†Permanent address: Département de Physique, Faculté des Sciences et Techniques, Université Sidi Mohamed Ben Abdellah, B.P. 2202, Fès 30000, Morocco.

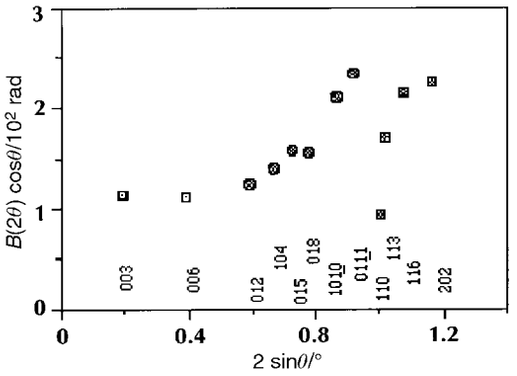

Fig. 1 Williamson–Hall plot for small-crystallite [Zn–Al–Cl].

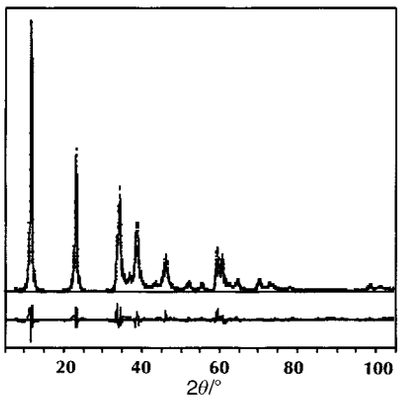

Fig. 2 Experimental, calculated and difference powder XRD patterns for [Zn–Al–Cl].

instrument. Ultra-thin sections (<100 nm) were prepared by embedding the crystals in a resin, followed by sectioning on an ultramichrotome fitted with a diamond knife. The thin sections were then picked up on uncoated copper grids.

Results and discussion

Analysis of line widths

As a preliminary stage, useful information can be obtained by comparison of the somewhat inaccurate values of the half-width, $B(2\theta)$, for several reflection groups. This is a recommended procedure before any more detailed analysis of size or size/strain broadening effects. The variation of $B(2\theta)$ with *hkl* is best displayed by means of a Williamson–Hall plot,[24] in which $B(2\theta)\cos\theta$ is reported as a function of $2\sin\theta$. Such a diagram (Fig. 1) immediately gives qualitative information about the size and shape of the crystallite and the presence or absence of lattice strain. The main feature displayed by this diagram is the separation of the experimental points in several series based on common (*hkl*) generic formula:

(1) The widths of the (003) and (006) lines are almost identical indicating that the lattice strain in the [00*l*] direction is negligible.
(2) The (110) line is the sharpest of all, indicating that the size is greater along this direction.
(3) For the (10*l*) lines, increasing width with increasing *l* Miller index is noticed with the corresponding points well aligned to a good approximation. If this set of lines was the only one observed on the PXRD, then it would have been concluded that the strain is the only effect of the broadening. However, this is not the case since similar behaviour is observed for the (11*l*) set. It can therefore be deduced that the lattice strain is negligible and that there is a marked anisotropy in the shape of coherent diffracting domains.

Structure refinement

It is well established that the structure of the 2-dimensional hydroxide layers of LDHs is very similar to that of brucite.[2,18,25] However, the distribution of the two types of cations is not fully understood. The structure is studied within the $R\bar{3}m$ space group, as isotypic to pyroaurite,[7] with a random distribution of metallic cations in the layers. The Cl^- anions and water molecules of interlayer domains are also considered to be statistically distributed. The site occupancies have been fixed according to the nominal composition.

A Rietveld refinement, using this set of atomic positions as a structural model, led to the reliability factors: $R_I = 8.19\%$ and

Table 1 Atomic and profile parameters for [Zn–Al–Cl]

Atom	Site1x(64)	Occupancy	*x*	*y*	*z*	B_{11}[a]/Å^2	B_{33}/Å^2	
Zn	3a	2/3		0.0	0.0	0.0	2.7(2)	4.7(4)
Al	3a	1/3		0.0	0.0	0.0	2.7(2)	4.7(4)
OH	6c	1		0.0	0.0	0.3775(1)	2.9(6)	5.7(3)
H_2O	18g	1/9		0.252(3)	0.0	0.5	18.0(4)	3.3(5)
Cl	18g	1/18		0.252(3)	0.0	0.5	18.0(4)	3.3(5)
Cell parameters/Å:			$a = 3.084(3)$			$c = 23.44(2)$		
Zero-shift, 2θ/°:			0.013(3)					
Profile parameters:[b]								
For "PH1"								
Size parameters:			$S_{11} = 0.154 \times 10^{-5}$			$S_{33} = 0.70(3) \times 10^{-5}$		
Strain parameters:			$D_{11} = 97.7(32)$			$D_{33} = 0.9(2)$		
K:			1.76(6)					
$\langle d' \rangle$/Å:			7.366					
For "PH2"								
Size parameters:			$S_{11} = 0.64(5) \times 10^{-4}$			$S_{33} = 0.93(3) \times 10^{-4}$		
Strain parameters:			$D_{11} = 8.5(3)$			$D_{33} = 0.10(5)$		
K:			1.44(8)					
$\langle d' \rangle$/Å:			7.366					
Asymmetry parameters:			$X_{11} = 0.041(3)$			$X_{33} = 0.9(1) \times 10^{-3}$		
Reliabilities (%):			$R_I = 4.41$			$R_P = 12.67$		
			$R_{WP} = 13.15$			$R_E = 2.80$		

[a] $B_{11} = B_{22} = 2B_{12}$; $B_{13} = B_{23} = 0$. [b] $S_{11} = S_{22} = 2S_{12}$; $S_{13} = S_{23} = 0$. $D_{11} = D_{22} = 2D_{12}$; $D_{13} = D_{23} = 0$. $X_{11} = X_{22} = 2X_{12}$; $X_{13} = X_{23} = 0$.

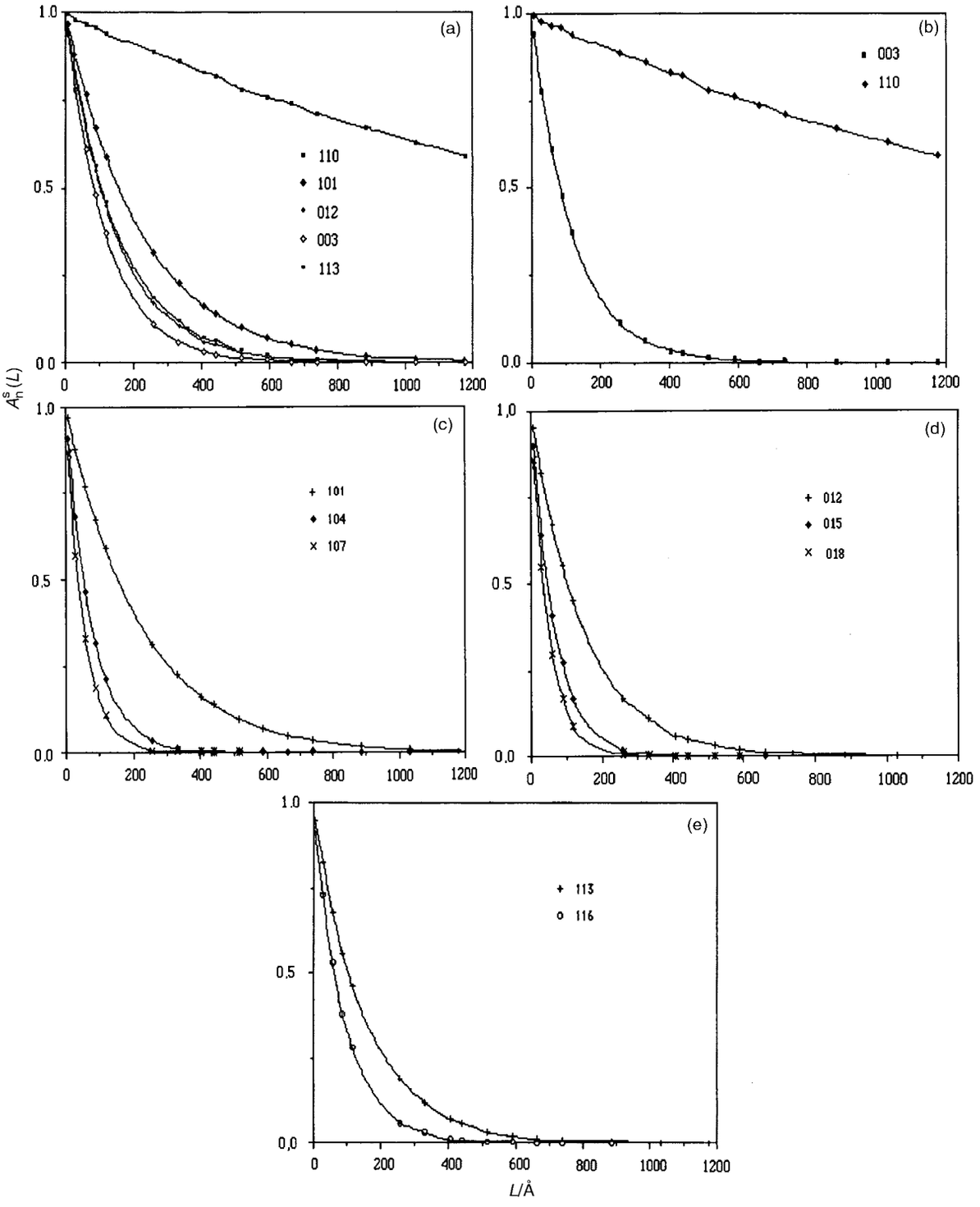

Fig. 3 Fourier cosine coefficients A^s_n *versus* L for small-crystallite [Zn–Al–Cl].

$R_{WP}=18.32\%$. At this stage, indications of anisotropic PXRD line broadening were noticed. The features evidenced on the Williamson–Hall diagram led us to examine the PXRD data using the "size–strain analysis" options of the modified Rietveld method (see ref. 26 and references therein). The refinement was performed by taking into account anisotropic and asymmetric PXRD line broadening. The instrumental profile g was determined from a well-crystallised ZnO sample measured under the same conditions; the true sample experimental profile of [Zn–Al–Cl] was then reproduced from the convolution product $h=f\times g$, where h is the experimental profile, by means of Fourier coefficients. Assuming a given distribution (Cauchy), an adjustable strain variation in space, and using an ellipsoid in order to approximate the mean coherency domain and the mean strain, the "Multi-pattern" option of the program was used in order to fit separately the profiles of the various categories of reflections. Two "virtual" phases were defined:

(1) A first phase (PH1) with lines widened by size and symmetrical strain effects. It was constituted of the (00*l*) and (110) lines.

(2) A second phase (PH2) with all the remaining lines, which are widened by size and asymmetric strain effects.

The experimental, calculated, and difference diffraction

Table 2 Interatomic distances (Å) and angles (°)

Distances	
(Zn,Al)–OH	2.060(2)
$(OH–OH)_{same\ layer\ side}$	3.084(4)
$(OH–OH)_{opposite\ vertices}$	4.120(4)
$(OH–OH)_{shared\ edges}$	2.732(5)
$(H_2O,Cl)–(H_2O,Cl)_{interlayer–interlayer}$	2.778(5)
$(H_2O,Cl)–OH_{layer–interlayer}$	2.975(6)
Angles	
$OH–(Zn,Al)–OH_{same\ layer\ side}$	96.9(2)
$OH–(Zn,Al)–OH_{shared\ edges}$	83.1(1)
$OH–(H_2O,Cl)–OH_{adjacent\ layers}$	149.7(4)

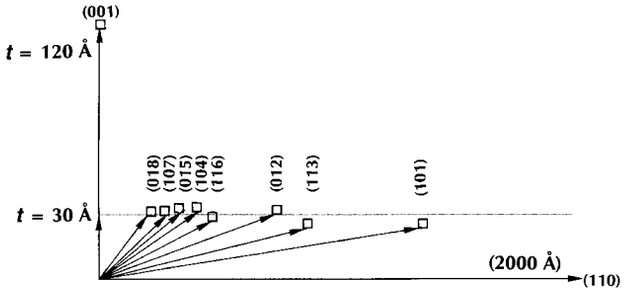

Fig. 4 Construction of shape of some crystallites of the phase based on the mean sizes.

patterns are shown in Fig. 2. The refinement results and atomic positions are reported in Table 1. A selection of interatomic distances is given in Table 2.

Description of structure

The structure, interatomic distances and angles are in good agreement with previous results for other LDHs. There was no evidence for a long range ordering of the metal cations in the layers which would give clear superstructure lines in relation with the strong difference of electronic density between Zn and Al.

The octahedral environment of metal cations is strongly distorted; the octahedra are flattened along the *c* axis as shown by the OH–(Zn,Al)–OH angles, which bring about short OH–OH distances in the shared octahedral edges. It has been found that the interlayer compression accounts virtually for the entire basal spacing contraction on increasing the Al concentration in [Mg–Al–CO_3] phases.[13] This is reflected in the strengthening of the hydrogen bonds between the layers and the interlayer domains, as has already been observed using IR spectroscopy by Miyata[27] and Hernandez-Moreno *et al.*[28] The interlayer domains are occupied by a disordered distribution of Cl^- ions and H_2O molecules. The layer–interlayer and interlayer–interlayer observed interatomic distances strongly suggest hydrogen bonding between these species. It is noteworthy that the atomic displacement factor in this interlayer domain is very anisotropic; $B_{11}=18$ Å^2 when $B_{33}=3.3$ Å^2. Similar behaviour was observed in the pyroaurite.

Analysis of size and strain parameters

The mean particle size and the strain parameters, *i.e.* the distribution of atomic positions around their equilibrium positions, are reported in Table 2. A small coherent size domain was observed. This is generally found in cold-worked materials.[26,29] It is believed that clear domain boundaries do not really exist but that the loss of coherency is progressive and related to lattice strain. The result for [Zn–Al–Cl] must probably be interpreted in the same way. For the "virtual" phase PH1, the sizes are of 119 Å and 2225 Å along the [00*l*] and [110] directions, respectively. It is noteworthy that the strain along the [00*l*] direction is much larger than along the [110] direction, which is consistent with the size effect. The $K=1.76$ value, which reflects the strain evolution *vs.* the distance, indicates that the shape profile associated with strain is intermediate between a Gaussian ($K=2$) and a Lorentzian ($K=1$) but is closer to the Gaussian profile. This result would be in agreement with an interpretation of the homogeneous coherency diffracting domains as corresponding to the mean separation between strain and dislocations or other defects. Indeed, the size effect is put in evidence by the representation $A^s_n(L)$ in the [00*l*] and [110] directions (Fig. 3b).

Concerning the "virtual" phase PH2, the effect of size is found to be anisotropic while that of the strain is isotropic (Table 3). The value of $K=1.44$ indicates that the profile shape associated with strain is intermediate between Gaussian and Lorentzian.

The Fourier coefficients *versus* distance curves are given in Fig. 3 for the characteristic reflections. It is immediately shown that there is a significant difference in the evolution of $A^s_n(L)$ coefficients corresponding to different reflections and that the crystallites are thus highly anisotropic. Furthermore, for (10*l*), (01*l*) and (11*l*) reflections, the initial slope increases with *l* (Fig. 3c,d,e), indicating that the form is probably parallelepipedic. Thus, the shape of the crystallites can be evaluated by a geometric construction (Fig. 4) from the values of the mean size calculated along different crystallographic directions (Table 3). The projection of the diffraction vectors [*hkl*] ($l\neq0$) along the [00*l*] direction perpendicular to the stacking direction of the layers is approximately constant. The corresponding thickness was of the order of $t'=30$ Å. This is definitely very low compared to the mean size obtained for the [00*l*] direction ($t=119$ Å) (Fig. 4). Such a difference is probably due to a loss of coherency along [*hkl*] ($l\neq0$) directions due to greater size anisotropy. This result is compatible with crystallites of plate-like shape with their size and thickness being of 2200 Å and 120 Å, respectively. According to the crystal symmetry of the solid, their cross section perpendicular to the [00*l*] directions is hexagonal.

Table 3 Mean size *M* (Å) and strain values in some characteristic directions

	Directions perpendicular to (*hkl*) planes									
	001	101	104	107	012	015	018	110	113	116
M^a/Å	119(5)	222(11)	77(6)	52(2)	135(6)	65(2)	48(2)	2225	152(6)	85(3)
$\langle Z_1'^2\rangle \times \langle d'^2\rangle \times 10^{2b}$/Å^2	10.5(12)	10.1(4)	10.2(4)	10.2(4)	10.0(4)	10.3(4)	10.4(3)	5.4(3)	10.1(4)	10.1(4)

^aM is related to the "surface" distribution while another definition $M1$ exists for a "volume" distribution (obtained from integral breadth for instance). When the size effect is fixed as a Cauchy-like broadening, the relation $1=2M$ is valid. $^b\langle Z_n'^2\rangle$ is obtained from $\langle Z_1'^2\rangle$ by the relation $\langle Z_n'^2\rangle = |n|K\langle Z_1'^2\rangle$, where $\langle Z_n'^2\rangle$ and K are refinable parameters ($K=1.76(6)$ for PH1 and $K=1.44(8)$ for PH2; $\langle d\rangle = 7.366$ Å, method reported in ref. 26).

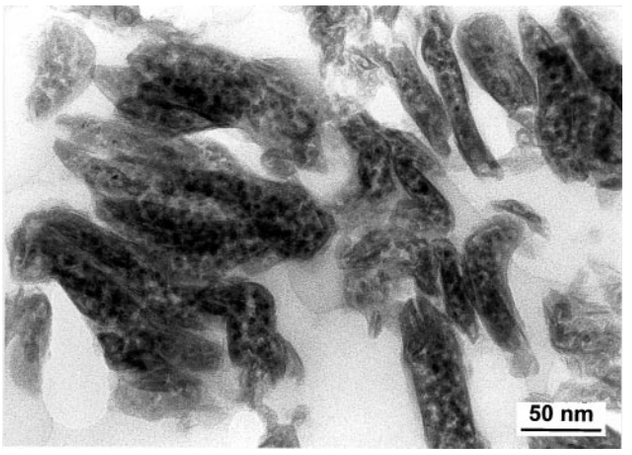

Fig. 5 TEM micrograph showing the morphological characteristics of [Zn–Al–Cl] crystallites.

TEM observations

TEM observations (Fig. 5) showed that the sample appeared to be constituted of crystallites with the typical plate morphology. The layered structure and the symmetry of the network forced the most developed faces to lie parallel to the brucite-like layers. This thickness of the crystallites corresponds therefore to the stacking of the layers along the stacking direction, which is perpendicular to the [00*l*] direction. The shape of some observed plates is more or less regular. It is likely that the irregular intragranular shapes are produced when the sample is subjected to the electron beam. Despite this limitation, the TEM results are in good agreement with those obtained by analysis of PXRD line broadening. The effective dimensions of the crystallites, as determined from the TEM micrographs, were found in the order of $2000 \times 2000 \times 200$ Å.

Conclusions

The analysis of the PXRD patterns of [Zn–Al–Cl], obtained by the salt–oxide method, can be explained by the existence of two kinds of lines: those widened by size and symmetrical strain effects and those widened by size and asymmetrical strain effects. Using the multi-pattern version of the Rietveld program, the structure of the studied phase was obtained by derivation from that of brucite. The cations are surrounded by hydroxides constituting octahedra, which share edges to form 2-dimensional layers. These octahedra are distorted as indicated by the OH–(Zn,Al)–OH bond angles and their flattening brings about short OH–OH distances in the shared octahedral edges. The strain and size of the crystallites were also obtained from the widths of the PXRD lines. These effects are treated as anisotropic, although the final result shows that this character is very marked for size with regard to strain. The mean particle size changes from 120 Å to 2200 Å in the [001] and [110] directions respectively, in good agreement with the results obtained by TEM observations.

References

1 A. De Roy, C. Forano, K. El Malki and J. P. Besse, in *Synthesis of Microporous Materials*, ed. M. L. Occelli and H. E. Robson, Van Nostrand Reinhold, New York, 1992, p. 108.
2 R. Allmann, *Chimia*, 1970, **24**, 99.
3 S. Miyata, *Clays Clay Miner.*, 1980, **28**, 50.
4 S. Miyata, *Clays Clay Miner.*, 1983, **31**, 305.
5 W. T. Reichle, *Solid State Ionics*, 1986, **22**, 135.
6 R. Allmann and H. H. Lohse, *Neues Jahrb. Mineral. Monatsh.*, 1966, 161.
7 R. Allmann, *Acta Crystallogr.*, 1968, **24**, 972.
8 M. C. Gastuche, G. Brown and M. Mortland, *Clay Mineral.*, 1967, **7**, 177.
9 G. Brown and M. C. Gastuche, *Clay Mineral.*, 1967, **7**, 193.
10 V. A. Drits, T. N. Sokolova, G. V. Sokolova and V. I. Cherkashin, *Clays Clay Miner.*, 1987, **35**, 401.
11 A. Ennadi, M. Khaldi, A. De Roy and J. P. Besse, *Mol. Cryst. Liq. Cryst.*, 1994, **244**, 373.
12 A. V. Besserguenev, A. M. Fogg, R. J. Francis, S. J. Price, D. O'hare, V. P. Isupov and B. P. Tolochko, *Chem. Mater.*, 1997, **9**, 241.
13 M. Bellotto, B. Rebours, O. Clause, J. Lynch, D. Bazin and E. Elkaim, *J. Phys. Chem.*, 1996, **100**, 8527.
14 P. Dumas, N. Ea, J. C. Niepce and G. J. Watelle, *J. Solid State Chem.*, 1979, **27**, 317.
15 J. C. Niepce, M. T. Mesnier and D. Louër, *J. Solid State Chem.*, 1977, **22**, 341.
16 H. M. Rietveld, *Acta Crystallogr.*, 1968, **2**, 65.
17 A. Le Bail, 10th Coll. Rayons X, Siemens, Grenoble, 1985.
18 B. E. Warren, *Prog. Metal. Phys.*, 1958, **8**, 147.
19 B. E. Warren and B. L. Averbach, *J. Appl. Phys.*, 1950, **21**, 595.
20 H. P. Bohem, J. Steinle and C. Vieweger, *Angew. Chem., Int. Ed. Engl.*, 1977, **16**, 265.
21 A. De Roy, J. P. Besse and P. Bondot, *Mater. Res. Bull.*, 1985, **20**, 1091.
22 K. El Malki, A. De Roy and J. P. Besse, *Eur. J. Solid State Inorg. Chem.*, 1989, **26**, 339.
23 M. F. McMurdie, M. C. Morris, E. H. Evans, B. Paretzkin, W. Wong-Ng and C. R. Hubbard, *Powder Diffract.*, 1986, **1**, 40.
24 G. K. Williamson and W. H. Hall, *Acta Metall.*, 1953, **1**, 22.
25 H. F. W. Taylor, *Mineral. Mag.*, 1973, **39**, 377.
26 C. Lartigue, A. Le Bail and A. Percheron-Guegan, *J. Less-Common Metals*, 1987, **129**, 65.
27 S. Miyata, *Clays Clay Miner.*, 1975, **23**, 369.
28 M. J. Hernandez-Moreno, M. A. Ulibarri, J. L. Rendon and J. S. Serna, *Phys. Chem. Miner.*, 1985, **12**, 34.
29 C. Greaves, *J. Appl. Crystallogr.*, 1985, **18**, 48.